

Tunable emission properties of CdSe/CdS quantum dots by Ce doping

Wonwoo Jeong^a, K.S. Hui^{b,*}, K.N. Hui^{c,*}, Young-Rae Cho^{a,*}, Kyung Mox Cho^a

^aSchool of Materials Science and Engineering, Pusan National University, San 30 Jangjeon-dong, Geumjeong-gu, Busan 609-735, Republic of Korea

^bSchool of Mathematics, University of East Anglia, Norwich, NR4 7TJ, United Kingdom

^cInstitute of Applied Physics and Materials Engineering, University of Macau, Avenida da Universidade, Macau, China

*Corresponding author:

E-mail: k.hui@uea.ac.uk (Kwan San Hui)

E-mail: bizhui@umac.mo (Kwun Nam Hui)

E-mail: yescho@pusan.ac.kr (Y. R. Cho)

Abstract

A facile one-step hydrothermal synthesis to prepare cerium (Ce^{3+}) ion doped CdSe/CdS core/shell quantum dots (QDs) is introduced. The effect of Ce^{3+} ion doping on structural and optical properties of the CdSe/CdS core/shell QDs is comprehensively investigated. With increasing Ce doping concentration, a linear increase in the lattice parameter is observed, suggesting the successful coupling of Ce^{3+} ions to the CdSe/CdS QDs. X-ray photoelectron spectroscopy reveals strong peaks of the Ce^{3+} state, indicating that Ce is initially present mainly in the Ce^{3+} ion state. In addition, red-shift over the range 538 to 569 nm is observed in the photoluminescence (PL) spectra of Ce^{3+} ion doped CdSe/CdS QDs. Results clearly indicates that the PL peak positions of the CdSe/CdS QDs could be controlled by the Ce content. This study highlights a new approach to tune the emission of the QDs.

Keywords: CdSe; CdSe/CdS; Ce dopant; Quantum dots; Tunable emission

1. Introduction

Semiconductor dots (QDs) have attracted significant attention in optoelectronic and electronic applications such as light-emitting diodes, solar cells, biological imaging, and nonvolatile memory owing to their appealing optical and electronic properties that can be controlled by the size quantization effect [1-4]. Among the semiconductor QDs, cadmium selenium (CdSe) QDs are widely studied because of its high luminescence quantum yield [5], and their tunable emission in the visible range tuned [6]. However, the luminescence of the QDs are prone to be affected by the surface, and interface structure due to more atoms are at the surface at such high surface-to-volume ratio [7, 8]. Accordingly, passivating the surface of the CdSe QDs with a shell of high bandgap CdS to form core/shell CdSe/CdS QDs has been demonstrated as a

promising approach to improve the luminescence and quantum yield of the CdSe QDs. As a result, high emission efficiency with 94% increase in quantum yield in the visible region was reported [9, 10].

Recently, studies have shown that new optical and magnetic properties can be realized by doping rare earth elements in CdSe QDs. For example, Martin-Rodriguez et al. reported the incorporation of Yb³⁺ in CdSe QDs resulting in a strong infrared emission at 1000 nm and extending the long lifetime of the Yb³⁺ emission [11]. Li et al. demonstrated Gd³⁺ doped in CdSe QDs exhibiting a high proton longitudinal relaxivity, which is promising for integrating systems for cellular imaging in biomedical applications [12]. As cerium (Ce) is one of the most studied elements in the lanthanide series owing to a simple energy level structure, a propensity to capture both electrons and holes, and the existence of Ce³⁺ or Ce⁴⁺ valence states [13]. However, the optical properties of doping Ce³⁺ in CdSe/Cds QDs are not well studied. Here we report a simple one-step hydrothermal approach to synthesize Ce³⁺ doped CdSe/Cds QDs. The effects of Ce³⁺ ion doping on the microstructural and optical properties of CdSe/CdS QDs are comprehensively examined. Decrease in band gap was confirmed by ultraviolet-visible spectroscopy, and the red-shift in the photoluminescence measurements was observed. In addition, PL emission at 549 nm corresponding to $^2D(5d) \rightarrow ^2F_{7/2}(4f)$ the transition of the Ce³⁺ ion was observed when the Ce concentration reached 4 mol.%. Results clearly demonstrate that the emission spectra of Ce³⁺ doped CdSe/CdS QDs could be tuned from 538 nm to 569 nm by changing the Ce³⁺ doping concentration.

2. Experimental

2.1 Materials

Cadmium chloride hemipentahydrate ($\text{CdCl}_2 \cdot 2.5\text{H}_2\text{O}$, 79.5-81%), sodium selenite (Na_2SeO_3 , 99-99.75%), 3-mercaptopropionic acid (MPA, 99%), and sodium borohydride (NaBH_4 , 98%) were purchased from Alfa Aesar. Cerium nitrate hexahydrate ($\text{Ce}(\text{NO}_3)_3 \cdot 6\text{H}_2\text{O}$, 99.5%) was obtained from Sigma-Aldrich (USA). All chemicals were used as received.

2.2 Synthesis of Ce-doped CdSe/CdS QDs

Ce-doped CdS/CdSe QDs were grown by a facile hydrothermal method following the reported method [14, 15]. In the first step, 2 mM $\text{CdCl}_2 \cdot 2.5\text{H}_2\text{O}$ as the Cd^{2+} source and 0, 0.02, 0.04, 0.06, 0.08, 0.1 mM $\text{Ce}(\text{NO}_3)_3 \cdot 6\text{H}_2\text{O}$ (0-5 mol.% compared to the Cd^{2+} content) were dissolved in 100 mL of DI water, and 3 mM MPA (as a stabilizer, molecular linker and S^{2-} source) was then added with continuous stirring. The pH was regulated to 10.5 with a 5 M NaOH solution. Third, 1 mM Na_2SeO_3 (as Se^{2+} source) and 2.65 mM NaBH_4 (as reductant) solutions were added in the above solution with stirring. The mixture was sealed in a 50 mL Teflon-lined stainless steel autoclave and kept in an oven at 150 °C for 45 min. After the hydrothermal process, the products were centrifuged at 5000 rpm for 30 min in ethanol to remove chemical residue, and the resulting products were obtained by vacuum filtration. The samples were labeled, 0.45Ce/CdSeCdS, 0.57Ce/CdSeCdS, 0.70Ce/CdSeCdS, 0.90Ce/CdSeCdS, and 1.01Ce/CdSeCdS, based on the corresponding various Ce loading in the CdSe/CdS QDs (Table 1).

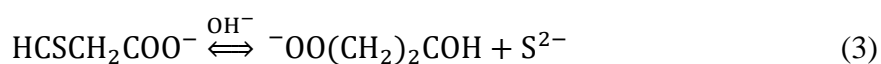
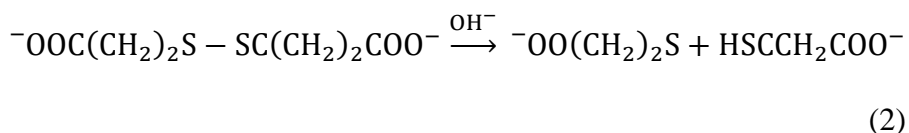
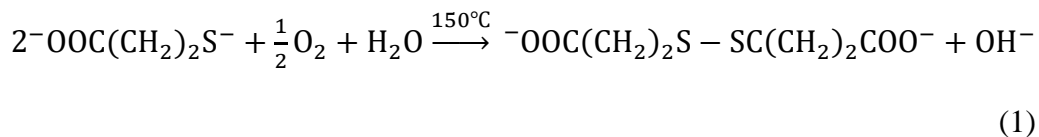
2.3 Characterization

X-ray powder diffraction (XRD) patterns were collected on a Rigaku MPA-2000 X-ray diffractometer with Cu $k\alpha$ radiation ($\lambda = 1.5418 \text{ \AA}$) at 40 kV voltage and a current of 40 mA. X-ray photoelectron spectroscopy (XPS) measurements were performed via the Thermo VG Escalab 250 photoelectron spectrometer. The morphology and chemical composition were characterized using a HITACHI S-4800 field emission scanning electron microscope (FESEM) equipped with an electron dispersive X-ray (EDX) spectrometer. High-resolution transmitting electron microscopy (HR-TEM) and selected-area electron diffraction (SAED) was performed using a JEM-2000F transmission electron microscope at an accelerating voltage of 200kV. For TEM sample preparation, one drop of ultrasonically-diluted nanoparticles suspended in absolute ethanol was placed on a carbon-coated copper grid and allowed to dry in air. The Raman spectra of the samples were recorded at room temperature using a Jobin-Yvon Horiba HR800 UV Raman microscope with an Ar⁺ laser ($\lambda=514.432 \text{ nm}$, 3.9 mW). Photoluminescence (PL) spectra were measured with He-Cd laser ($\lambda=325.01 \text{ nm}$, 0.06 mW). The absorption spectra were obtained by UV-Visible spectroscopy Agilent HP8453 in the wavelength range 350 - 800 nm.

3. Results and discussion

The synthesis of the Ce-doped CdSe/CdS core/shell QDs is illustrated in Fig. 1. Initially, at low temperature ($\leq 100 \text{ }^\circ\text{C}$) Na₂SeO₃ was firstly reduced by NaBH₄ to provide an air-stable Se²⁺ source to form the CdSe core [14, 16]. Because S²⁻ anions were released very slowly through the decomposition of MPA at low temperature during the synthesis, only Ce-doped CdSe monomers were nucleated as seeds. During the synthesis of CdSe core, Ce ions were doping into the lattice of the CdSe core. When reaction temperature reaches 150 °C, sufficient amounts

of S²⁻ anions will be released from MPA to grow the CdS shell on the CdSe core. The reaction mechanism of formation of CdS shell using MPA is proposed as follows [17]:



As the reaction goes on, more Se²⁻ anions are consumed and the growth of CdS was dominated at the final stage, resulting in the proposed Ce-doped CdSe/CdS core/shell QDs.

Fig. 2 reveals the XRD pattern of Ce-doped CdSe/CdS QDs. The diffraction peaks are matched with the cubic CdSe (JCPDS 88-2346) and CdS (JCPDS 89-0440) phases, indicating the successful formation of CdSe/CdS QDs. The crystallite size (*D*) of the CdSe/CdS QDs was calculated using the Scherrer equation:

$$D = \frac{k\lambda}{\beta \cos\theta} \quad (4)$$

where *k* is a constant equal to 0.94, *λ* is the wavelength of the incident X-rays, *θ* is the diffraction angle of the peak in radians, and *β* is the full width at half-maximum (FWHM) of the peaks. With increasing Ce dopant concentration from 0 to 5 mole%, (111) peak shifted to lower 2*θ*, indicating the increase of the *d* spacing. The average crystal size of the Ce-doped CdSe/CdS QDs was calculated to be 4.16, 4.20, 4.22, 4.27, 4.30, 4.64 nm. The increasing

crystallite size was attributed to the nucleation and subsequent growth rate with increasing Ce doping [18] and the substitution of Ce^{3+} (1.01 Å) for Cd^{2+} (0.95 Å) [19].

Fig. 3a shows the energy dispersive X-ray spectroscopy of the 1.01Ce/CdSeCdS QDs revealing the presence of elements Cd, Se, S, and the dopant Ce in the sample. To understand how the substitution of Ce^{3+} ions was taken place at the Cd sites of the CdSe/CdS QDs, Vegard's law empirical analysis is employed to predict the structural effects of dopant and investigate the statistical substitution of a guest ion (Ce^{3+} ion) into the host lattice (Cd site) with increasing Ce^{3+} ion concentration [20, 21]. Using Vegard's law, structural effects of the Ce doping in CdSe/CdS QDs is revealed by plotting the change in lattice parameter as a function of Ce dopant concentration. Fig. 3b shows a shift in the *a*-lattice parameter of Ce-doped CdSe/CdS QDs with increasing Ce ions mole ratio. The observed linear enlargement of *a*-lattice expansion of approximately 1.1% from 599.2 to 605.7 pm with increasing Ce dopant concentration is in accordance with the predictions of Vegard's law, suggesting that Ce^{3+} doping occurs at the Cd lattice sites in the CdSe/CdS QDs.

Fig. 4 shows the XPS analysis of Ce 3d spectra that consists of a mixed valence state of Ce^{3+} and Ce^{4+} . It was reported that the Ce 3d spectra could be assigned to two sets of spin-orbital multiplets, i.e., $3d_{5/2}$ and $3d_{3/2}$ which are denoted as v and u in Fig. 4, respectively [22]. The v_0 , v' and u_0 , u' peaks are attributed to the two main and satellite peaks of the Ce^{3+} state, respectively, while the v , v'' , v''' and u , u'' , u''' peaks are attributed to the three main and satellite

peaks of the Ce^{4+} state, respectively. The peaks between 880-895 eV correspond to Ce $3d_{5/2}$, while the peaks between 895-910 eV correspond to Ce $3d_{3/2}$ and peak at 917.4 eV is a characteristic satellite peak indicating the presence of +4 state [23]. Strong peaks for the Ce^{3+} state are visible in the XPS Ce 3d spectrum of the sample, indicating that Ce is initially present mainly in the Ce^{3+} state.

Fig. 5 (a) shows SEM image of the 1.01Ce/CdSeCdS sample possessing homogeneous QDs. Fig. 5 (b)-(d) show high-resolution TEM (HRTEM) images of the undoped and Ce-doped CdSe/CdS QDs. These QDs exhibit an almost spherical shape with a uniform particle size, and the inserts show the QDs exhibiting a good crystal structure. In addition, the observed lattice fringes in the HRTEM images suggest crystalline structure with ABCABC stacking cubic structure. Moreover, no segregation of Ce-rich particles was observed by HRTEM, which suggests that Ce^{3+} or Ce^{4+} ions are incorporated into the CdSe/CdS QDs. The diameters of the undoped CdSe/CdS QDs, 0.70Ce/CdSeCdS, and 1.01Ce/CdSeCdS QDs were estimated to be 4.6 nm, 4.9 nm and 5.2 nm, respectively. HRTEM images indicate that QDs exhibits a relatively narrow size distribution with a relative standard deviation of 13-16%. Compared to the CdSe/CdS QDs, the Ce doped CdSe/CdS QDs exhibits larger particle sizes, which matches well with XRD data (Fig. 2) and Vegard's law (Fig. 3b).

Fig. 6 presents the Raman spectrum of Ce-doped CdSe/CdS QDs with different Ce concentrations. The peaks of the undoped CdSe/CdS QDs located at 197.5 cm^{-1} and 279.3 cm^{-1}

¹ (marked as LO1 and LO2) were assigned to the scattering of CdSe and CdS longitudinal optic phonons, respectively [24]. In addition, higher-order Raman peaks were also observed at 395.3 cm⁻¹ and the other mode at 477.3 cm⁻¹, revealing a second-order phonon frequency of CdSe mode masked as 2LO1. Remarkably, CdSe- and CdS-like phonon peaks (LO_{CdSe}+LO_{CdS}) are observed at 477.3 cm⁻¹, which is the sum of $\omega_{LO1}=197.5$ and $\omega_{LO2}=279.3$ cm⁻¹. Similar studies conducted by Lu et al. [25] and Dzhagan et al. [24] reported the existence of the CdSe_xS_{1-x} phases at the interface of the CdSe/CdS QDs. Furthermore, the peak positions of LO1 and 2LO1 are shifted towards the higher frequency, whereas the peak position of LO2 is shifted towards a lower frequency, which might attribute to the increase of grain sizes CdSe/CdS QDs with increasing Ce mole ratio [25-28].

Fig. 7 shows the typical UV-visible absorption spectra of the Ce-doped CdSe/CdS QDs. The absorption spectrum of the undoped CdSe/CdS QDs (black solid line) exhibited an absorption onset at 551 nm (2.25 eV) followed by an excitonic peak centered at 522 nm (2.37 eV) as well as a long absorption tail above 590 nm. The absorption onset was determined from the dip in the first derivative (marked with a circle in Fig. 7) [29] and the excitonic peak was obtained by fitting the absorption curve to two Gaussian bands [30] (plotted as dashed lines). In addition, the excitonic peak was assigned to the characteristic transition for the first excitonic state (1S_e1S_{3/2}) of the CdSe QDs [31].

With increasing the Ce dopant concentration, the photoluminescence (PL) emission peak shifted gradually from 538 nm (2.30 eV) to 569 nm (2.18 eV), which was accompanied by a red shift in the absorbance peak from 521 nm to 552 nm (Fig. 8). The Stokes shift is the overall red shift of emission peak compared to the absorbance peak, i.e., the emitted photon has less energy than the absorbed photon. The emission peaks are closely aligned with the edge of the corresponding absorption spectrum, confirming the band-edge emission of these QDs. Besides, the optical band gaps of undoped and Ce-doped CdSe/CdS QDs were in the range of 2.30-2.18 eV, which are higher than their bulk counterpart (1.7 eV) [32]. The observed higher optical band gap in QDs compared to the bulk material was attributed to the quantum confinement effect due to the localization of electrons and holes in the QDs causing a change in the electronic band structure [33]. In addition, the red shift in the PL emission could be related to the decrease in band gap due to the change in particle size with increasing Ce content. Meulenberg et al. [20] reported the red-shift in the PL emission in the Cu-doped CdSe QDs was attributed to the sub-gap trap states from the dopants. When the Ce dopant concentration is higher than 3 mol.%, two emission peaks were observed at 549 nm and 565 nm in the 0.90Ce/CdSeCdS and 1.01Ce/CdSeCdS QDs. The main emission peak at 565 nm was assigned to the emission of CdSe/CdS core/shell QDs, whereas the shoulder peak at 549 nm was attributed to the transition of the Ce³⁺ ion from the lowest components of the 5d state to the ²F_{7/2} components of the ground state [34]. Zhu et al. reported the PL emission shoulder at 550 nm from a CaS:Ce phosphor for the lowest state ²F_{7/2} of the single 4f electron of Ce³⁺ [35].

4. Conclusion

Ce-doped CdSe/CdS core/shell QDs were synthesized by a facile one-step hydrothermal route. XRD showed that Ce doping does not lead the formation of any secondary phase precipitate in the studied Ce dopant concentration range of 0-5 mol.%. XRD and HRTEM confirmed that the size of QDs increased with increasing Ce dopant concentration. XPS confirmed the chemical state of the Ce³⁺ ions in the CdSe/CdS QDs. The band gaps of the Ce-doped CdSe/CdS QDs showed a blue shift with increasing Ce dopant concentration due to the larger grain size with increasing Ce mole ratio as well as the quantum confinement effect. In addition, PL results showed that the peak position could be tuned easily from 538 nm to 569 nm by changing the Ce dopant concentration. In particular, the emission peak at 549 nm is attributed to the Ce dopants concentration. This study provides a simple and promising strategy for tuning the emission spectrum of CdSe/CdS QDs by incorporating lanthanide ions.

Acknowledgements

This work was supported by the UEA funding.

References

- [1] F. Wang, R.R. Deng, J. Wang, Q.X. Wang, Y. Han, H.M. Zhu, X.Y. Chen, X.G. Liu, *Nat. Mater.*, **10**, 968-973, (2011)
- [2] O. Chen, J. Zhao, V.P. Chauhan, J. Cui, C. Wong, D.K. Harris, H. Wei, H.S. Han, D. Fukumura, R.K. Jain, M.G. Bawendi, *Nat. Mater.*, **12**, 445-451, (2013)
- [3] L. Etgar, D. Yanover, R.K. Capek, R. Vaxenburg, Z.S. Xue, B. Liu, M.K. Nazeeruddin, E. Lifshitz, M. Gratzel, *Adv. Funct. Mater.*, **23**, 2736-2741, (2013)
- [4] K.W. Han, M.H. Lee, T.W. Kim, D.Y. Yun, S.W. Kim, S.W. Kim, *Appl. Phys. Lett.*, **99**, 193302, (2011)
- [5] K. Surana, P.K. Singh, H.W. Rhee, B. Bhattacharya, *J. Ind. Eng. Chem.*, **20**, 4188-4193, (2014)
- [6] Y.L. Lee, B.M. Huang, H.T. Chien, *Chem. Mater.*, **20**, 6903-6905, (2008)
- [7] A. Eychmuller, *J. Phys. Chem. B*, **104**, 6514-6528, (2000)
- [8] A.P. Alivisatos, *J. Phys. Chem.*, **100**, 13226-13239, (1996)
- [9] W.G. Chang, Y.H. Shen, A.J. Xie, H. Zhang, J. Wang, W.S. Lu, *J. Colloid Interface Sci.*, **335**, 257-263, (2009)
- [10] X.G. Peng, M.C. Schlamp, A.V. Kadavanich, A.P. Alivisatos, *J. Am. Chem. Soc.*, **119**, 7019-7029, (1997)
- [11] R.G. Rosa Martin-Rodriguez, and Andries Meijerink, *J. Am. Chem. Soc.*, **135**, 13668-13671, (2013)
- [12] I.F. Li, C.S. Yeh, *J. Mater. Chem.*, **20**, 2079-2081, (2010)
- [13] N.R. Panda, B.S. Acharya, T.B. Singh, R.K. Gartia, *J. Lumin*, **136**, 369-377, (2013)

- [14] J. Wang, H.Y. Han, *J. Colloid. Interf. Sci.*, **351**, 83-87, (2010)
- [15] K.N. Hui, K.S. Hui, X.L. Zhang, R.S. Mane, M. Naushad, *Sol. Energy*, **125**, 125-134, (2016)
- [16] H.F. Qian, L. Li, J.C. Ren, *Mater. Res. Bull.*, **40**, 1726-1736, (2005)
- [17] H.F. Qian, X. Qiu, L. Li, J.C. Ren, *J Phys Chem B*, **110**, 9034-9040, (2006)
- [18] P.U. Gitanjali Dhir, N.K. Verma, *Mater. Sci. Semicond. Process.*, **27**, 611-618, (2014)
- [19] R.D.Shannon, *Acta Crystallogr.*, **A32**, 751-767, (1976)
- [20] R.W. Meulenberg, T. van Buuren, K.M. Hanif, T.M. Willey, G.F. Strouse, L.J. Terminello, *Nano Lett.*, **4**, 2277-2285, (2004)
- [21] O.E. Raola, G.F. Strouse, *Nano Lett.*, **2**, 1443-1447, (2002)
- [22] T. Naganuma, E. Traversa, *Nanoscale*, **4**, 4950-4953, (2012)
- [23] C. Korsvik, S. Patil, S. Seal, W.T. Self, *Chem. Commun.*, DOI 1056-1058, (2007)
- [24] V.M. Dzhagan, M.Y. Valakh, A.E. Raevskaya, A.L. Stroyuk, S.Y. Kuchmiy, D.R.T. Zahn, *Nanotechnology*, **18**, 285701, (2007)
- [25] L. Lu, X.L. Xu, W.T. Liang, H.F. Lu, *J. Phys.: Condens. Matter* **19**, 406221 (2007)
- [26] V.M. Dzhagan, M.Y. Valakh, A.E. Raevskaya, A.L. Stroyuk, S.Y. Kuchmiy, D.R.T. Zahn, *Nanotechnology*, **19**, 305707, (2008)
- [27] L.B. Hai, N.X. Nghia, P.T. Nga, V.D. Chinh, N.T.T. Trang, V.T.H. Hanh, *J. Exp. Nanosci.*, **4**, 277-283, (2009)
- [28] S. Chandramohan, A. Kanjilal, S.N. Sarangi, S. Majumder, R. Sathyamoorthy, C.H. Hong, T. Som, *Nanoscale*, **2**, 1155-1159, (2010)

- [29] J. Planelles-Arago, E. Cordoncillo, R.A.S. Ferreira, L.D. Carlos, P. Escribano, J. Mater. Chem., **21**, 1162-1170, (2011)
- [30] J. He, W. Ji, G.H. Ma, S.H. Tang, H.I. Elim, W.X. Sun, Z.H. Zhang, W.S. Chin, J. Appl. Phys., **95**, 6381-6386, (2004)
- [31] E.A. McArthur, A.J. Morris-Cohen, K.E. Knowles, E.A. Weiss, J. Phys. Chem. B, **114**, 14514-14520, (2010)
- [32] K. Singh, S.S.D. Mishra, Sol. Energ. Mat. Sol. C, **71**, 115-129, (2002)
- [33] Z.M. Yuan, P. Yang, Mater. Res. Bull., **48**, 2640-2647, (2013)
- [34] V. Kumar, S.S. Pitale, V. Mishra, I.M. Nagpure, M.M. Biggs, O.M. Ntwaeaborwa, H.C. Swart, J. Alloy Compd., **492**, L8-L12, (2010)
- [35] V. Singh, T.K.G. Rao, J.J. Zhu, M. Tiwari, Mat Sci Eng B-Solid, **131**, 195-199, (2006)

Figure and Table captions

Fig. 1. Schematic diagram of Ce-doped CdSe/CdS core/shell QDs synthesized using a one-step hydrothermal method.

Fig. 2. XRD patterns of Ce-doped CdSe/CdS QDs with different Ce doping concentration.

Fig. 3. (a) Energy dispersive X-ray spectrum of 1.01Ce/CdSeCdS sample; (b) Vegard's law plot of the lattice parameter mole fraction of dopant for Ce-doped nanocrystals.

Fig.4. Ce $3d_{5/2, 3/2}$ XPS spectrum of 1.01Ce/CdSeCdS sample fitted with ten peaks, including satellites, corresponding to Ce^{3+} and Ce^{4+} .

Fig. 5. (a) SEM images of 1.01Ce/CdSeCdS. HRTEM images of Ce-doped CdSe/CdS QDs with Ce mole fractions of (b) 0, (c) 0.03 and (d) 0.05. Top right insert: HRTEM images of particles with lattice fringes corresponding to (111) planes. Bottom right insert: TEM diffraction imaging.

Fig. 6. Raman spectra of Ce-doped CdSe/CdS QDs with different Ce content.

Fig. 7. UV- visible absorption spectra for Ce-doped CdSe/CdS QDs with various Ce dopant concentrations (solid line). Absorption spectra of undoped CdSe/CdS QDs fitted to two Gaussian bands (dashed line) to locate the excitonic peak (522 nm). The circle in the experimental spectrum indicates the absorption onset (551 nm).

Fig. 8. The photoluminescence spectra of Ce-doped CdSe/CdS QDs with various Ce dopant concentrations.

Table 1 Elemental composition of the samples by EDX analysis.

Table 1

Sample	Ce (at%)	Cd (at%)	Se (at%)	S (at%)	O (at%)	Ce loading (mole%)
0.45Ce/CdSeCdS	0.45	40.95	29.17	18.16	11.27	1
0.57Ce/CdSeCdS	0.57	41.37	28.46	17.68	11.92	2
0.70Ce/CdSeCdS	0.70	40.12	29.15	17.86	12.17	3
0.90Ce/CdSeCdS	0.90	39.98	27.85	18.55	12.71	4
1.01Ce/CdSeCdS	1.01	39.06	26.62	19.82	13.49	5

Fig. 1

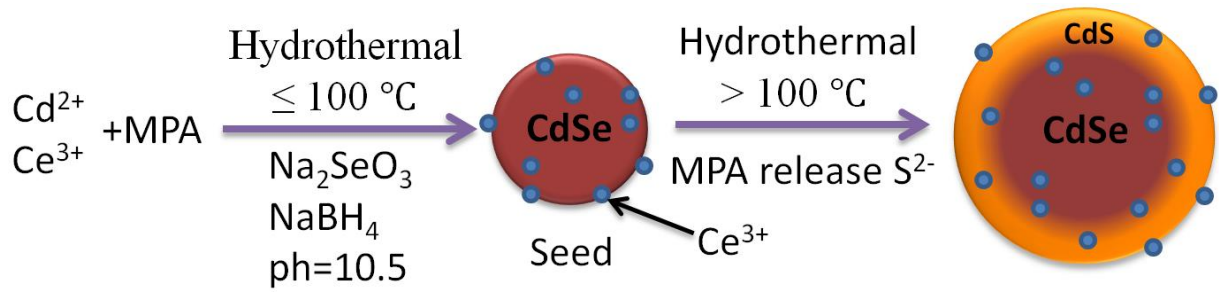


Fig. 2

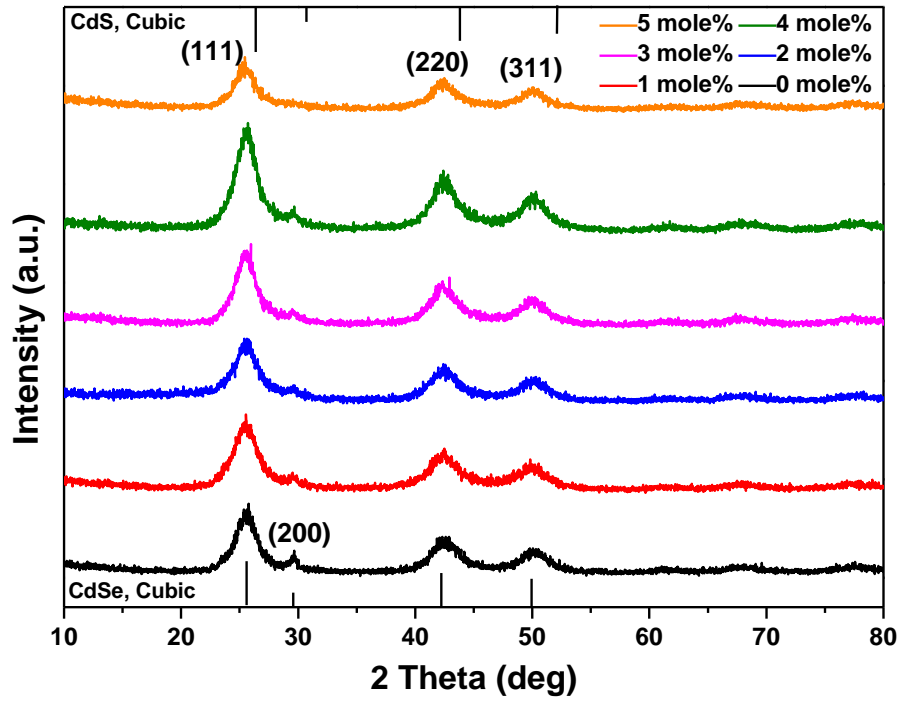


Fig. 3

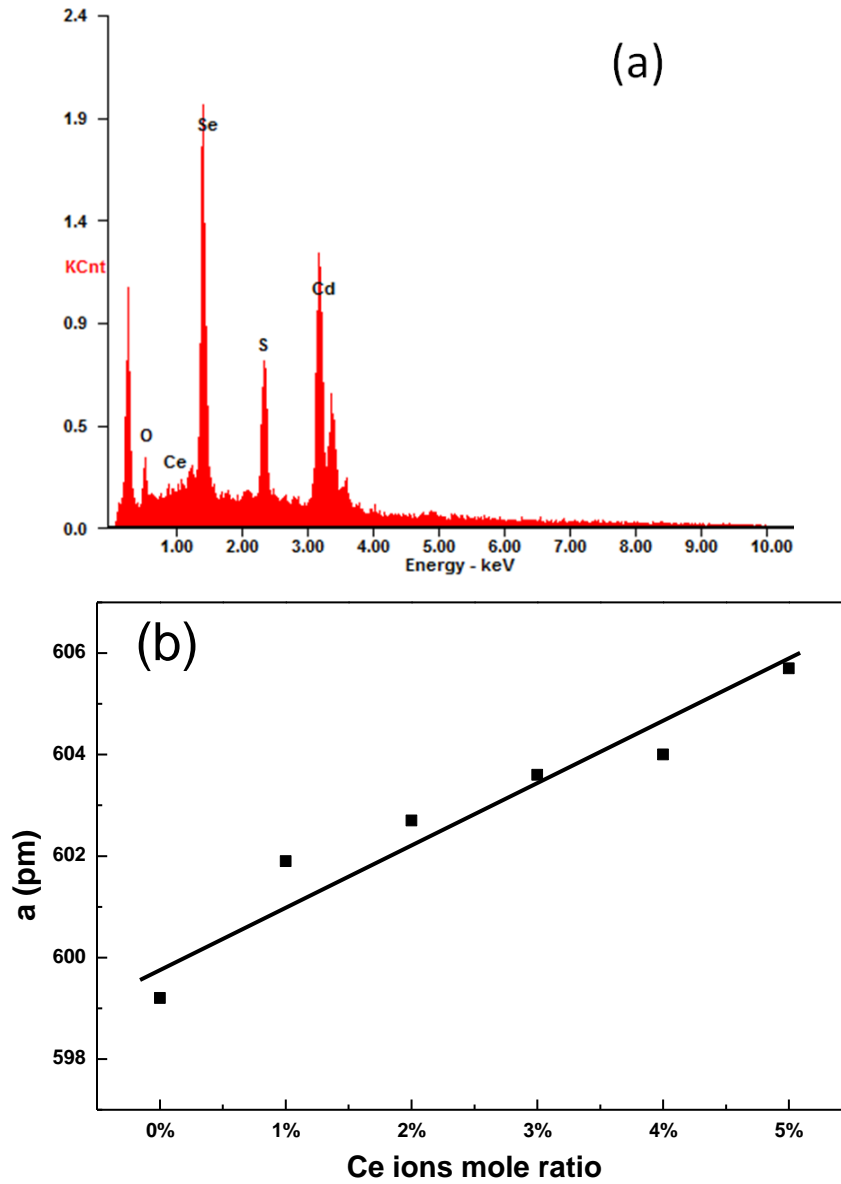


Fig. 4

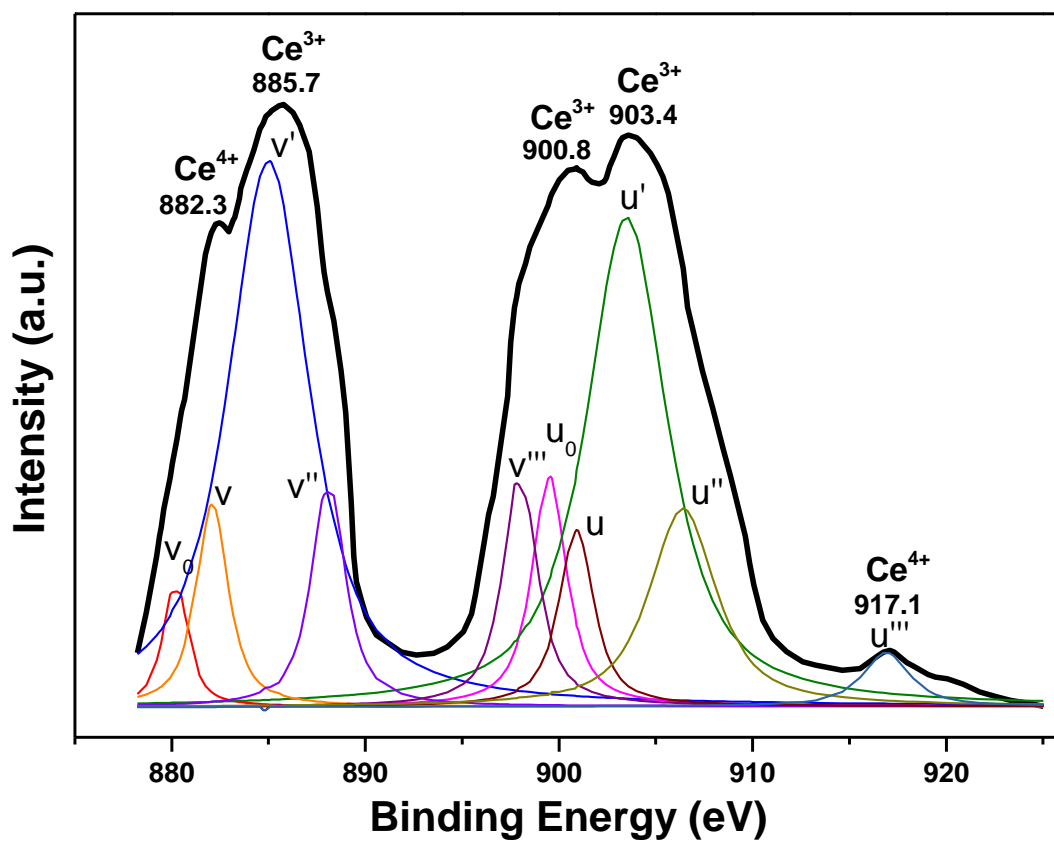


Fig. 5

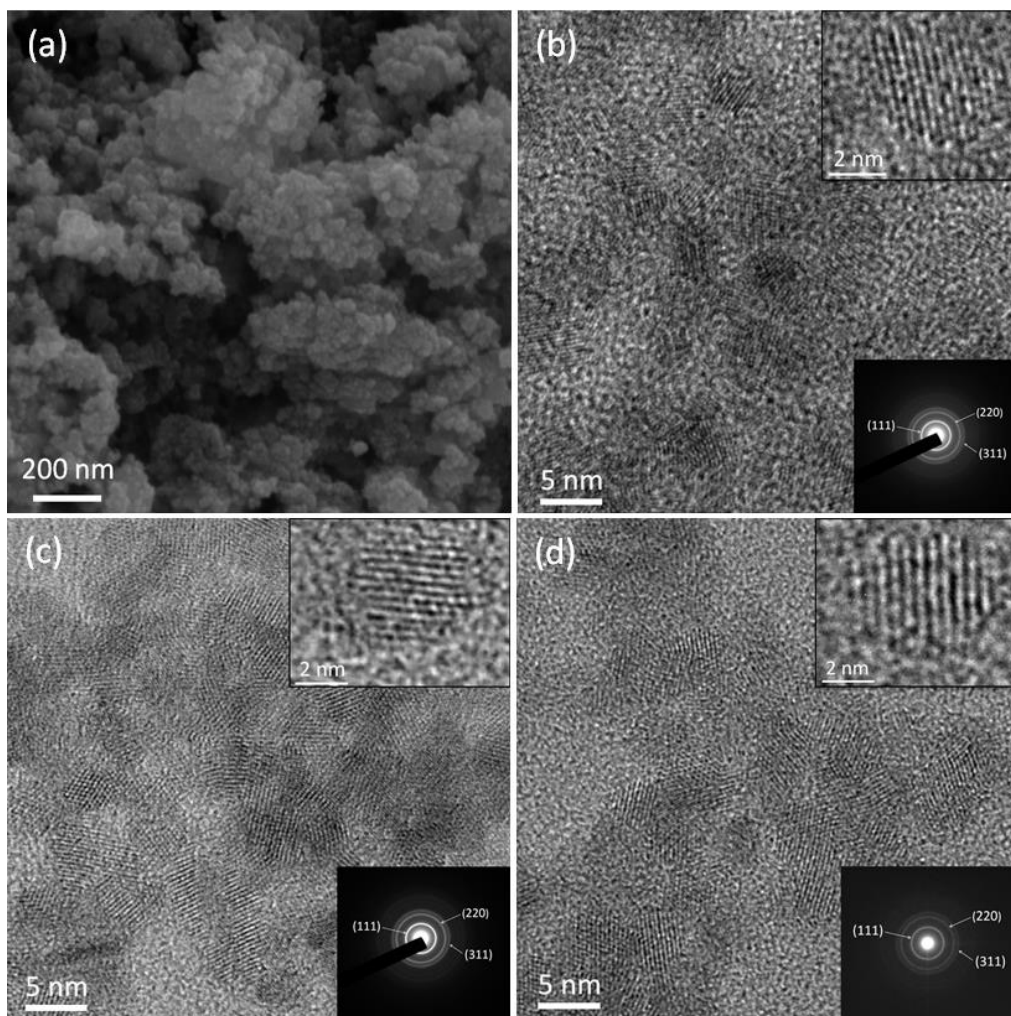


Fig. 6

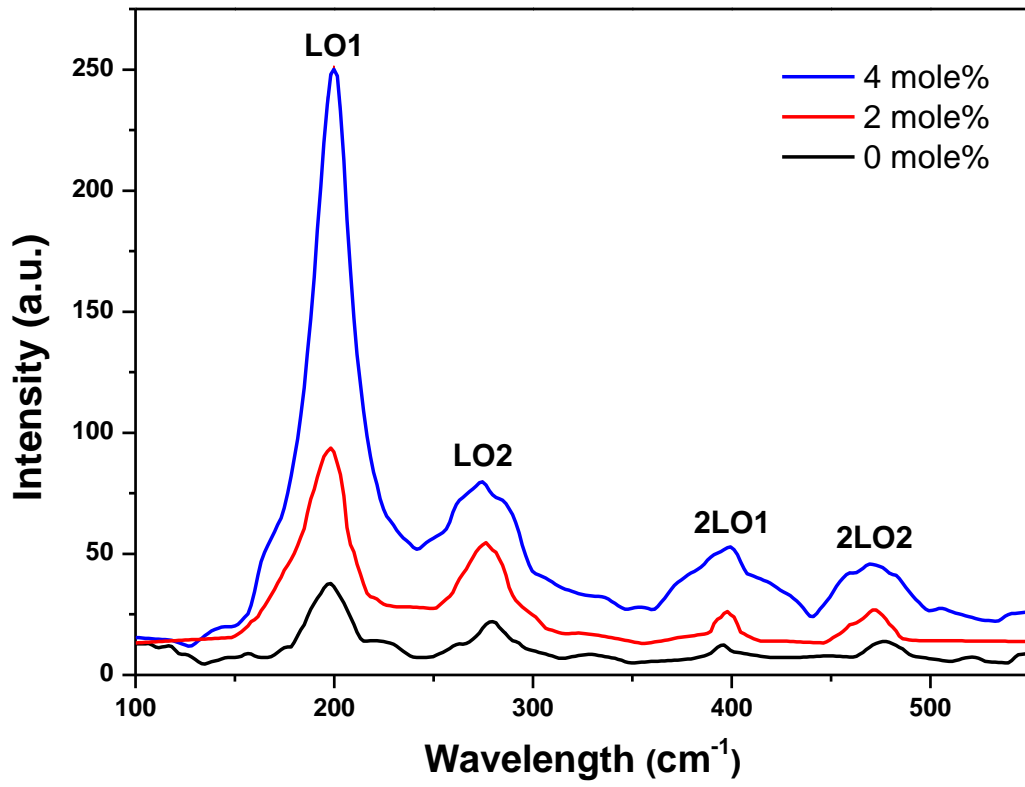


Fig. 7

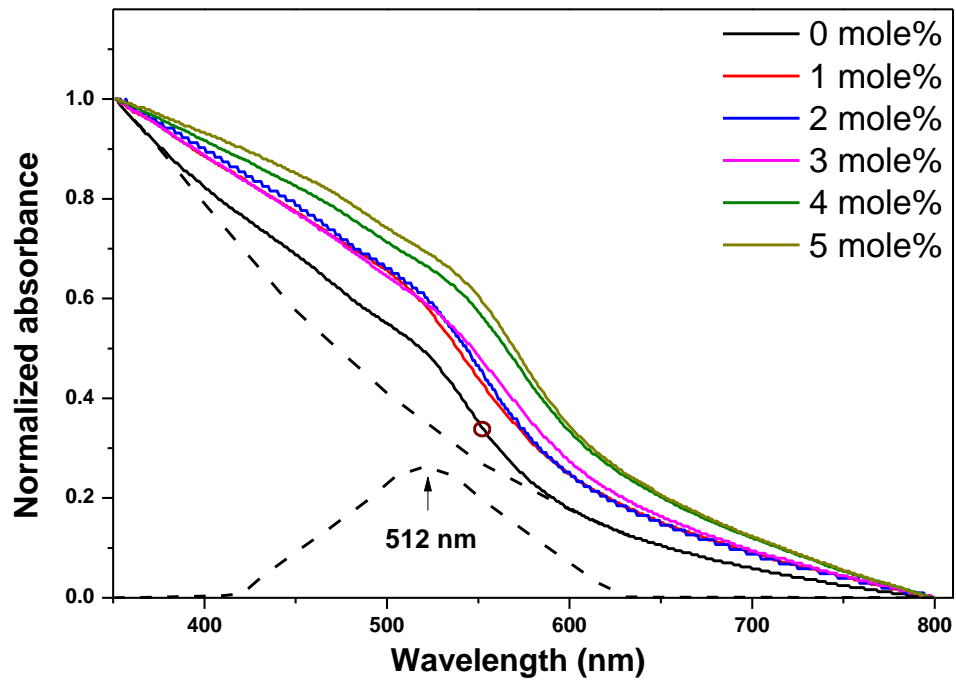


Fig. 8

